A NOVEL APPROACH TO MEASURING METHANE DIFFUSIVITY THROUGH A HYDRATE FILM USING DIFFERENTIAL SCANNING CALORIMETRY

Simon R. Davies, Jason W. Lachance, E. Dendy Sloan, Carolyn A. Koh*

Center for Hydrate Research
Colorado School of Mines, CO 80401
USA

ABSTRACT

The avoidance of hydrate blockages in deepwater subsea tiebacks presents a major technical challenge with severe implications for production, safety and cost. The successful prediction of when and where hydrate plugs form could lead to substantial reductions in the use of chemical inhibitors, and to corresponding savings in operational expenditure. The diffusivity of the gas hydrate former (methane) or the host molecule (water), through a hydrate film is a key property for such predictions of hydrate plug formation.

In this paper, a novel application of Differential Scanning Calorimetry is described in which a hydrate film was allowed to grow at a hydrocarbon-water interface for different hold-times. By determining the change in mass of the hydrate film as a function of hold-time, an effective diffusivity could be inferred. The effect of the subcooling, and of the addition of a liquid hydrocarbon layer were also investigated. Finally, the transferability of these results to hydrate growth from water-in-oil emulsions is discussed.

Keywords: Diffusivity, DSC, Hydrate Film Growth

NOMENCLATURE

C Dimensionless methane concentration in the aqueous phase [-]
C_A Methane concentration in the aqueous phase [kg m^{-3}]
C_{Ai} Methane concentration in the aqueous phase in equilibrium with hydrate [kg m^{-3}]
C_{A0} Initial concentration of methane in the aqueous phase before hydrate formation [kg m^{-3}]
D_A Diffusivity of methane in water [m^2 s^{-1}]
Film Thickness of the hydrate film [m]
iend Total number of grid points [-]
m Mass of methane in the hydrate film [kg]
n An integer [-]
t Time [s]
x Distance [m]
X Dimensionless distance [-]
Z A function depending only on x
δ Thickness of the hydrate film and water layer [m]
ε Porosity of hydrate layer [m^3m^{-3}]
ε_0 Initial porosity of hydrate layer [m^3m^{-3}]
θ A function depending only on t
ξ A constant [-]
π Pi [-]
φ Dummy variable for integration [s]

INTRODUCTION

As the oil and gas industry moves into deeper water and corresponding higher pressures from larger liquid heads, the risk of hydrate formation is increasing. Recent research has focused on the rate of formation of a hydrate plug, in addition to the traditional research on hydrate avoidance. The

* Corresponding author: Phone: +1 303 273 3237 Fax +1 303 273 3730 E-mail: ckoh@mines.edu

conceptual picture for hydrate formation in water-in-oil (W/O) emulsions is shown in Figure 1 [1].

There are two critical interrelated steps in the formation of a plug: hydrate growth and hydrate agglomeration. Hydrate growth is the focus of this paper.

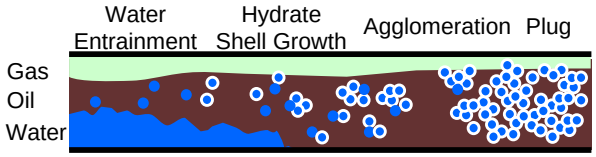

Figure 1: A Conceptual Picture for Hydrate Formation in Water-in-Oil (W/O) Emulsions

Upon nucleation, a hydrate film rapidly forms around the water droplets; this process is limited by heat transfer, both for CO_2-water systems [2], [3] and for methane-water systems [4]. The various heat transfer models have been summarized by Mochizuki and Mori [5]. After the film has formed completely, the growth rate transitions from a heat transfer limited process to a process limited by mass transfer [2].

Guest molecules initially dissolved inside the water droplet can migrate to the hydrate film, as can water initially dissolved in the oil phase. At longer timescales the hydrate formation rate is limited by the mass transfer of the water [6] or guest molecule [7] through the hydrate film.

In this paper High Pressure Differential Scanning Calorimetry (HP-DSC) is applied to study mass transfer limitations to hydrate formation. A hydrate film was allowed to grow at a hydrocarbon-water interface for different hold-times. Assuming that the growth rate was controlled by the transport of methane across the film and using a quasi-steady state approximation (neglecting accumulation and hydrate growth inside pores or fissures within the film), the change of hydrate mass with time could be measured and used to infer an effective diffusivity.

The effect of the subcooling, and of the addition of a liquid hydrocarbon layer were also investigated. The transferability of these results was tested by comparison to the hydrate growth in a similar experiment with water-in-oil emulsions.

EXPERIMENTAL METHODOLOGY

Differential Scanning Calorimetry (DSC) is a widely used technique to study the thermal properties of a sample [8]. A Differential Scanning Calorimeter consists of a sample cell and a reference cell.

During an experiment, both cells are heated or cooled according to a pre-programmed temperature profile. The difference in heat flux required to obtain a zero temperature difference between the sample and reference cells can be analyzed to determine the thermal properties of the sample, such as specific heat capacity, or the latent heat associated with phase changes

In this paper, a High Pressure DSC was used (HP-micro DSC VII, Setaram Instruments, France). Ultra high purity methane (> 99.99 %,Airgas Inc.) and chromatography grade water (Aldrich Inc.) were used.

The experimental procedure is summarized in Figure 2. The DSC cell was first loaded with a known mass of water. The cell was then sealed, placed in the DSC and pressurized with methane. Pressures ranging from 30 to 150 bar have been investigated. A saturation period of 3 hours at 30°C was used to ensure that the water was fully saturated before hydrate formation occurred.

The sample was then cooled to an isotherm (-5 or -10°C), and hydrate was allowed to nucleate as indicated by an exotherm. Following a pre-determined hold period, the sample was then heated to dissociate the hydrate, as indicated by an endotherm. The exothermic and endothermic peaks could both be integrated to determine the mass of hydrate after the initial growth period and at the point of dissociation.

In order to understand the time dependence on the effective diffusivity, a series of identical experiments were performed with different hold times. The mass of hydrate as a function of time could then be determined from the full series of experiments.

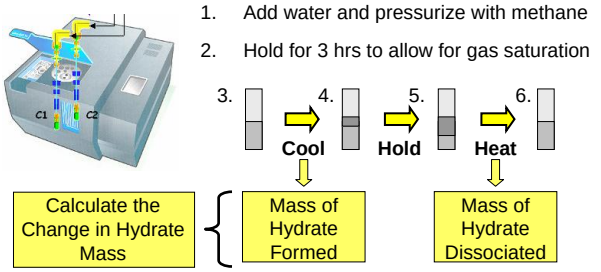

Figure 2: A Schematic Diagram Showing the Experimental Procedure for the HP-DSC Experiments

A typical thermogram for the DSC experiments is shown in Figure 3. The mass of hydrate initially formed, was found by integrating the exothermic formation heat-flux peak, and then dividing the energy by the latent heat of methane hydrate (446 J/g). The same procedure was followed for the dissociation peak. See the thesis by Lachance [9] for a more detailed explanation of the experimental procedure.

Since the formation conditions were below the ice point, ice formed instead of hydrate in some of the experiments. Ice nucleation was indicated by a much larger formation exotherm; all of the water phase converted to ice compared to only the gas-water interface for hydrate formation. In addition the melting endotherm would occur at 0°C on reheat. These results were omitted from this study. If ice did not nucleate before the hydrate then no ice formation occurred during the growth period. The presence of ice would have been indicated at the end of the experiment by an endotherm at 0°C during the reheat stage.

The hydrate nucleation at -10°C generally occurred earlier than at -5°C due to the larger subcooling [10]. In some experiments, the hydrate nucleated during the cooling step. The results from these experiments were omitted from this study due to the poorly defined formation temperature which may have influenced mass transfer across the film.

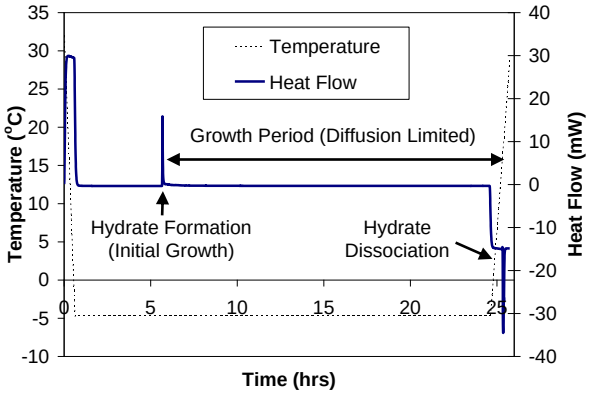

Figure 3: A Typical Thermogram from a Diffusivity Experiment in the HP-DSC

THEORY

A conceptual picture for the growth and annealing of the hydrate film is presented in Figure 4. From the experimental data it is apparent that the mass transfer resistance varies non-linearly with the film thickness. This suggests that mass transfer resistance increases as the hydrate ages.

Initially it is proposed that the hydrate forms as a homogeneous layer with a given porosity (ε_0). Over time the film porosity decreases as the pores fill.

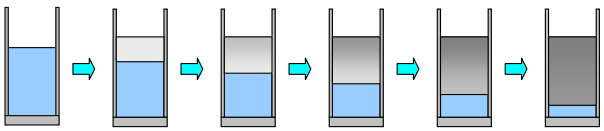

Figure 4: A Conceptual Picture of Hydrate Film Growth and Annealing (blue shading: water/gas system, grey shading: hydrate film)

There are two sources of methane for hydrate formation: the free water phase and the gas phase. Dissolved methane will diffuse from the water phase, initially saturated with methane, to the hydrate film over time. At the same time, methane from the free gas phase and water from the aqueous phase will diffuse through the hydrate film. All of these processes will cause pore filling and film growth. A schematic representation of the free methane concentration profile is shown in Figure 5.

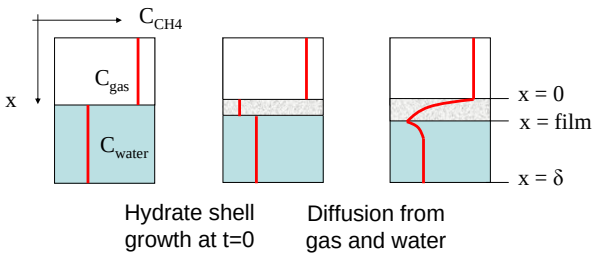

Figure 5: A Schematic Representation of the Free Methane Concentration Profile

The diffusivity of methane in water at 4°C is approximately 8.5 x 10^{-10} m^2/s [11]. The equilibrium methane concentrations in the aqueous phase with and without a hydrate phase were estimated using Multiflash with the Association Model (CPA-Infochem); the estimated concentrations are listed in Table 1.

	Methane Concentration In The Aqueous Phase at 150 bara (kg/m3)	
Temperature (°C)	In The Presence of Hydrate	Without Hydrate
-5	0.67	4.0
-10	0.50	4.5

Table 1: Methane Concentrations in the Aqueous Phase as Estimated by Multiflash

As already mentioned, there are two sources of hydrate formers to be considered: methane already dissolved in the water phase, and hydrate formers being transported across the hydrate film. In order to de-convolute the contribution to the film growth of dissolved methane from the mass transfer of water molecules or gas molecules across the hydrate film it is necessary to first model the methane diffusion in the free water phase. One-dimensional Fick's Law in rectilinear coordinates applies (Equation 1). Two solution procedures were applied: an analytical solution, and a numerical solution.

$$\frac{\partial C_A}{\partial t} = D_A \frac{\partial^2 C_A}{\partial x^2} \qquad \textbf{Equation 1}$$

Boundary Conditions:

$$C_A = C_{Ai} \qquad x = Film \qquad t \geq 0$$

$$\frac{\partial C_A}{\partial x} = 0 \qquad x = \delta \qquad t \geq 0$$

Initial Condition:

$$C_A = C_{A0} \qquad Film < x \leq \delta \qquad t = 0$$

Analytical Solution for the Free Water Phase

The partial differential equation (PDE) in Equation 1 can be split into two ordinary differential equations (ODE's) using the product method; the ODE's can then be solved with a Fourier series [12].

Since the closed boundary condition is problematic, it is convenient to solve the symmetrical problem (twice the distance): $\text{Film} < x < (2\delta\text{-Film})$. Only half of the solution is utilized. Using the dimensionless variable C, the revised initial conditions and boundary conditions are as follows:

$$C = 0 \qquad X = 0,1 \qquad t \geq 0$$

$$C = 1 \qquad 0 < X < 1 \qquad t = 0$$

Where:

$$C = \frac{C_A - C_{Ai}}{C_{A0} - C_{Ai}}$$

$$X = \frac{x - Film}{2(\delta - Film)}$$

The resulting ODEs from the product method are shown in Equation 2 and 3 where the term ζ is a constant and Z and θ are functions depending on only one variable.

$$\frac{d^2 Z}{dx^2} + \zeta Z = 0 \qquad \textbf{Equation 2}$$

$$\frac{d\theta}{dt} + \zeta^2 \theta D_A = 0 \qquad \textbf{Equation 3}$$

The solution of the PDE is provided by the Fourier series as shown in Equation 4.

$$C = \sum_{n=1}^{\infty} \frac{4e^{\frac{-(2n-1)^2 \pi^2 D_A t}{4(\delta - Film)^2}}}{\pi(2n-1)} \sin\left(\frac{(2n-1)\pi(x - Film)}{2(\delta - Film)}\right)$$

Equation 4

Numerical Solution for the Free Water Phase

The numerical solution of the PDE was found using the forward difference method [13]. The PDE is expressed in standard explicit form in Equation 5.

$$\frac{C_{t+\Delta t} - C_t}{\Delta t} = D_A \frac{C_{i+1} - 2C_i + C_{i-1}}{(\Delta x)^2} \qquad \textbf{Equation 5}$$

The closed boundary condition was imposed by equating the two grid points at the bottom of the cell:

$$C_{iend} = C_{iend-1} \qquad t \geq 0$$

The comparison of the analytical solutions for 1000 steps to the numerical solutions is shown in Figure 6. The agreement between both models is excellent. The Gibbs Phenomenon [14] is evident in the analytical solution at 0 minutes.

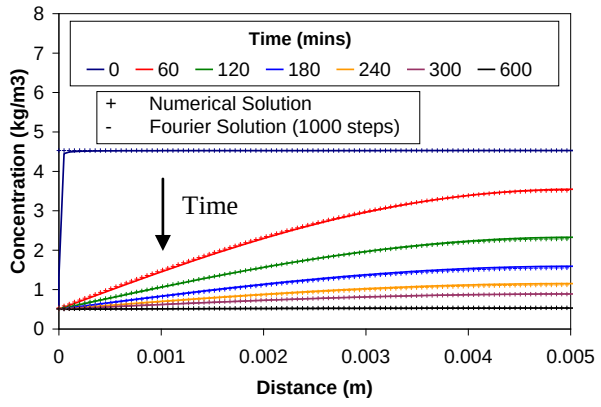

Figure 6: Comparison of the Analytical Solutions for 1000 Steps to the Numerical Solutions

RESULTS AND DISCUSSION

Before initiating experiments in the DSC it was necessary to pre-saturate the water phase with methane. The saturation was achieved by holding the pressurized DSC cell at 30°C for three hours in a methane atmosphere prior to cooling to the hydrate formation conditions.

Before the saturation procedure was implemented the mass of hydrate formed in the nucleation exotherm was stochastic. However, when the water had been pre-saturated, the results were reproducible:

- Standard Deviation. = 2 J/g for different samples
- Standard Deviation = 0.56 J/g for the same sample

Table 2 compares the experimental data obtained for various saturation periods. Less hydrate formed in the experiments before the saturation period of three hours was implemented. For the experiments given in Table 2, hydrate was formed at -5°C.

Saturation Period (hrs)	Dissociation Endotherm (J/g)
4.3	25.28
3.2	30.96
3	25.41
2.5	28.12
2.2	26.44
1.4	12.32
<1	13.44

Table 2: Comparison of Experimental Results Before and After the Pre-Saturation Procedure was Implemented

In order to study the mass of hydrate as a function of time, a series of repeat experiments were performed for different hold-times. The mass of hydrate at the end of each experiment was found from the dissociation endotherm. Two such experimental series are plotted in Figure 7 for isotherms of -5°C and -10°C.

The predicted mass of hydrate versus time for an impermeable hydrate layer (methane diffusing to the hydrate from the bulk water only) is plotted in the same figure for comparison. The mass of hydrate formed from dissolved methane was calculated by integrating the mass transfer rate

(Equation 6) over time at the hydrate boundary, as shown Equation 7. The concentration gradient in the x direction was found by differentiating Equation 4.

$$\frac{dm}{dt} = D_A A \frac{dC_A}{dx} \qquad \textbf{Equation 6}$$

$$m = \int_0^t D_A A \frac{dC_A}{dx} . d\varphi \qquad \textbf{Equation 7}$$

In the case of the experimental series at -10°C most of the hydrate formation could be attributed to methane that was initially dissolved in the water phase; little methane appears to have diffused through the hydrate film in the timescale of these experiments. However for the experimental series at -5°C, the mass of hydrate formed was significantly higher than could be attributed to dissolved methane alone; the film was more permeable to hydrate formers in this case.

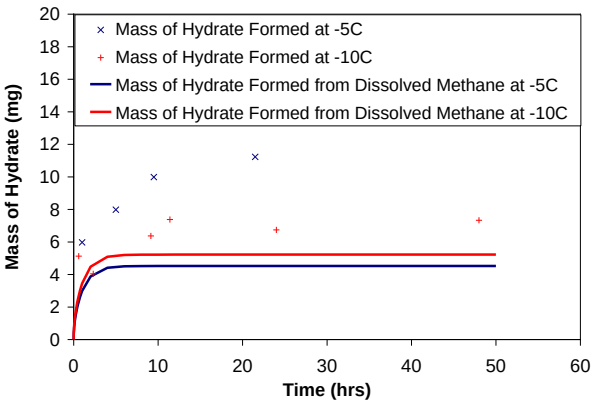

Figure 7: Mass of Hydrate Formed Versus Time at Various Subcoolings Compared to the Mass of Hydrate Formed from Dissolved Methane in Water

The addition of a liquid hydrocarbon layer on top of the water layer was found to greatly reduce the rate of hydrate formation, either as a result of the additional mass transfer resistance to gas molecules, or due to a less permeable hydrate film. In the experiments with a hydrocarbon layer, the hydrate growth could again be explained by methane dissolved in the water layer (See Figure 8).

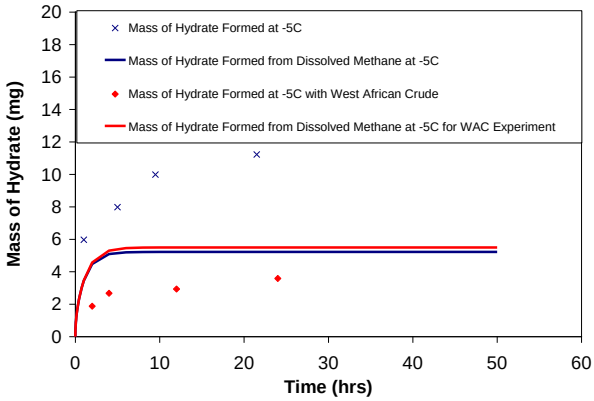

Figure 8: Mass of Hydrate Formed Versus Time for a West African Crude Layer above the Water Phase Compared to the Mass of Hydrate Formed from Dissolved Methane

A greater mass of hydrate formed at -5°C compared to -10°C. This is at first thought counter-intuitive and in contrast to previous work that shows increased hydrate growth with higher subcooling [15]. Figure 9 illustrates the hydrate growth at several subcoolings using the DSC.

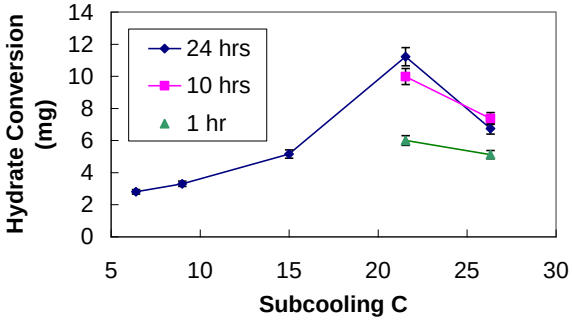

Figure 9: Hydrate Conversion with Various Subcoolings at Different Time Periods

The DSC results in Figure 9 confirm previously reported [15] trends, but additionally illustrate that at subcoolings greater than 20°C, the hydrate growth is impeded possibly due to the faster annealing of the film. This phenomenon was also found to occur in water-in-crude oil emulsions (Figure 10).

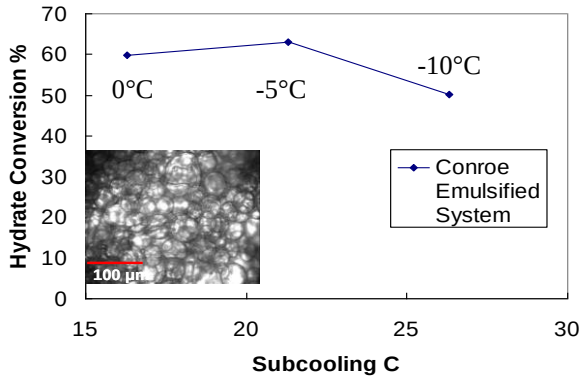

Figure 10: Hydrate Conversion in Water-In-Conroe Crude at Different Isotherms. Inset: Microscopic image of water-in-oil emulsion.

Conroe crude oil was used in the emulsion tests due to the large droplet sizes (Figure 10 inset) that did not fully convert to hydrate upon nucleation. Figure 10 shows the hydrate growth for different isotherms. Again, higher conversion was achieved at the -5°C isotherm than at the -10°C isotherm, as in Figure 7. However, the 0°C isotherm begins to follow the expected literature [15] trend that higher subcoolings result in more hydrate growth (*cf.* Figure 9 up to subcoolings of 20°C).

Estimating the Effective Diffusivity

In the film growth experiments (Figures 7 and 8), hydrate was allowed to form at the water interface. In the case of the experiment performed at -10°C, the mass of hydrate formed could be explained by methane initially dissolved in the water phase. However at -5°C, the hydrate growth was in excess of that which could be explained by dissolved methane. Assuming that the difference in the hydrate growth in these experiments could be attributed to the transport of methane across the film, an effective diffusivity could be regressed to the experimental data.

A quasi-steady state approximation was made for these calculations; accumulation of methane in the film was neglected, the thickening of the film and hydrate growth inside pores or fissures within the film was expected to be slow in comparison to the mass transport rate across the film. The one-dimensional steady state Fick's Law (Equation 6) therefore applied.

The mass of hydrate formed is the sum of that formed from dissolved methane and that formed from the mass transfer of methane across the hydrate film. The effective diffusivity of methane across the film was unknown and could be regressed to the experimental data using the least squares method (See Figure 11). The regressed effective diffusivity for the experiments at -5°C was 7.6×10^{-13} m^2/s; for the experiments at -10°C the effective diffusivity was 3.4×10^{-13} m^2/s.

However, it is apparent that the experimental observations and the predicted hydrate growth rates show markedly different trends. At short timescales the predictions under-predict and at longer timescales the predictions over-predict the hydrate growth rate. It appears that the effective diffusivity is time dependent, dropping off over time as the film anneals. This result coincides with the conceptual picture for hydrate film formation presented in Figure 4.

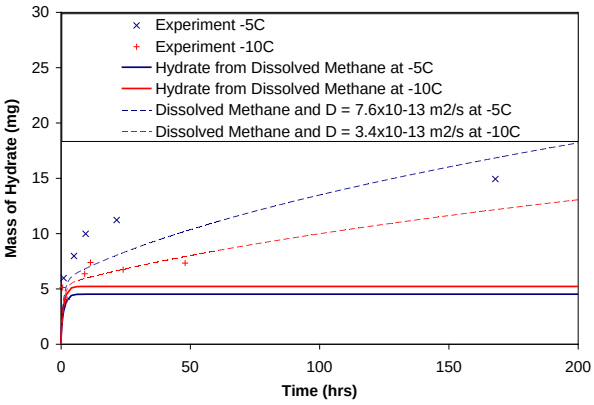

Figure 11: Mass of Hydrate Formed Versus Time for Various Subcoolings Compared to the Mass of Hydrate Formed from Dissolved Methane and the Best Fit Diffusivity through the Shell

CONCLUSIONS

Less permeable hydrate films form in the presence of a liquid hydrocarbon layer. The hydrate growth measured in these DSC experiments could be explained by methane initially dissolved in the aqueous phase.

The growth rate of hydrate was found to increase with sub-cooling until the temperature was reduced below approximately -5°C (20°C subcooling); at lower temperatures the growth rate was reduced.

This effect has been observed for pure water systems and for emulsified water-in-oil emulsions.

The effective diffusivity of methane through the hydrate shell was shown to decrease with time as the hydrate layer anneals and pores and fissures in the film fill.

ACKNOWLEDGEMENTS

The authors wish to acknowledge the financial support received from the CSM Hydrate Consortium of energy companies: BP, Champion, Chevron, ConocoPhillips, ExxonMobil, Halliburton, Petrobras, Schlumberger, Shell, and StatoilHydro.

REFERENCES

[1] Sloan E.D. and Koh C.A. *Clathrate Hydrates of Natural Gasses*, 3rd Ed., Chemical Industries 119, CRC Press, Taylor and Francis Group, Boca Raton, 2008.

[2] Uchida T., Ebinuma T., Kawabata J., Narita H. *Microscopic Observations of Formation Processes of Clathrate-Hydrate Films at an Interface between Water and Carbon Dioxide.* Journal of Crystal Growth, 1999; 204: 348-356.

[3] Mori Y.H. *Estimating the Thickness of Hydrate Films from Their Lateral Growth Rate Using a Simplified Heat Transfer Model.* Journal of Crystal Growth, 2001; 223: 206-212.

[4] Freer E.M., Selim M.S. and Sloan E.D. *Methane Hydrate Film Growth Kinetics.* Fluid Phase Equilibria, 2001; 185: 65-75.

[5] Mochizuki T. and Mori Y.H. Clathrate Hydrate Film Growth Along Water / Hydrate - Former Phase Boundaries – A Conductive Heat-Transfer Model. Proceedings of the 5th International Conference on Gas Hydrates, 1009, Vol. 1, pp64-74, Trondheim, Norway, 2005.

[6] Mori Y. and Mochizuki T. *Modeling of Mass Transport across a Hydrate Layer Intervening Between Liquid Water and "Guest" Fluid Phases.* Proceedings of the 2nd International Conference on Gas Hydrates, pp267-8274, Toulouse, France, 1996.

[7] Turner *D.J. Clathrate Hydrate Formation in Water-in-Oil Dispersions.* PhD Thesis, Colorado School of Mines, 2005.

[8] Dean, John A. *The Analytical Chemistry Handbook*. New York. McGraw Hill, Inc. pp. 15.1–15.5, 1995.

[9] Lachance J.W. *Investigation of Gas Hydrates Using Differential Scanning Calorimetry With Water-In-Oil Emulsions.* Masters Thesis, Colorado School of Mines, 2008.

[10] Hester K.C., Davies S.R., Lachance J.W., Sloan E.D. and Koh C.A. *Hydrate Nucleation Measurements using High Pressure Differential Scanning Calorimetry.* Proceedings of the 6th International Conference on Gas Hydrates, Vancouver, Canada, 2008.

[11] Witherspoon P.I. and Bonoli L. *Correlation of Diffusion Coefficients for Parafin, Aromatic and Cycloparafin Hydrocarbons in Water.* I & EC Fundamentals. 1969; 8(3): 589-591.

[12] Kreyszig E. *Advanced Engineering Mathematics.* 8th Edition, New York. Wiley Inc. p587-593. 1997.

[13] Von Rosenberg D.U. *Methods for the Numerical Solution of Partial Differential Equations.* Modern Analytic and Computational Methods in Science and Mathematics. No. 16, American Elsevier Publishing Company Inc. New York, p16-20, 1969.

[14] Thompson W.J. *Fourier Series and the Gibbs Phenomenon.* American Journal of Physics, 1992; 60(5): 425-429.

[15] Taylor *C.J. Adhesion Force Between Hydrate Particles And Macroscopic Investigation Of Hydrate Film Growth At The Hydrocarbon / Water Interface.* Masters Thesis, Colorado School of Mines, 2006.